

Document made available under the Patent Cooperation Treaty (PCT)

International application number: PCT/US2004/039339

International filing date: 22 November 2004 (22.11.2004)

Document type: Certified copy of priority document

Document details: Country/Office: US
Number: 60/524,074
Filing date: 21 November 2003 (21.11.2003)

Date of receipt at the International Bureau: 16 June 2007 (16.06.2007)

Remark: Priority document submitted or transmitted to the International Bureau in compliance with Rule 17.1(a) or (b)



World Intellectual Property Organization (WIPO) - Geneva, Switzerland
Organisation Mondiale de la Propriété Intellectuelle (OMPI) - Genève, Suisse



THE UNITED STATES OF AMERICA

TO ALL TO WHOM THESE PRESENTS SHALL COME:

UNITED STATES DEPARTMENT OF COMMERCE

United States Patent and Trademark Office

June 07, 2007

THIS IS TO CERTIFY THAT ANNEXED HERETO IS A TRUE COPY FROM THE RECORDS OF THE UNITED STATES PATENT AND TRADEMARK OFFICE OF THOSE PAPERS OF THE BELOW IDENTIFIED PATENT APPLICATION THAT MET THE REQUIREMENTS TO BE GRANTED A FILING DATE.

APPLICATION NUMBER: *60/524,074*

FILING DATE: *November 21, 2003*

RELATED PCT APPLICATION NUMBER: *PCT/US04/39339*

THE COUNTRY CODE AND NUMBER OF YOUR PRIORITY APPLICATION, TO BE USED FOR FILING ABROAD UNDER THE PARIS CONVENTION, IS *US60/524,074*



Certified by

Under Secretary of Commerce
for Intellectual Property
and Director of the United States
Patent and Trademark Office

11/21/03
60152 U.S. PTO
11/21/03

Re 05/03

PROVISIONAL APPLICATION COVER SHEET

This is a request for filing a PROVISIONAL APPLICATION under 37 CFR 1.53 (c).

MAIL STOP PROVISIONAL APPLICATION

Commissioner for Patents

P.O. Box 1450

Alexandria, VA 22313-1450

22387 U.S. PTO
60/524074
11/21/03

Docket Number: BU-110Xq800		Type a Plus sign (+) inside this box →	+
INVENTOR(s)/APPLICANT(s)			
LAST NAME	FIRST NAME	MIDDLE INITIAL	RESIDENCE (CITY AND EITHER STATE OR FOREIGN COUNTRY)
Li	Biao		Brighton, MA
Zhang	Xin		Boston, MA
Bifano	Thomas		Mansfield, MA
Sharon	Andre		Newton, MA
<input type="checkbox"/> Additional Inventors are being named on Page 2 attached.			
TITLE OF THE INVENTION (280 characters max)			
UNCOOLED CANTILEVER MICROBOLOMETER FOCAL PLANE ARRAYS WITH mK TEMPERATURE RESOLUTIONS			
CORRESPONDENCE ADDRESS			
<input checked="" type="checkbox"/> Customer Number 207		which is associated with the Law Firm of: WEINGARTEN, SCHURGIN, GAGNEBIN & LEOVICI LLP Ten Post Office Square Boston, Massachusetts 02109 United States Telephone: (617) 542-2290 Fax: (617) 451-0313	
ENCLOSED APPLICATION PARTS (CHECK ALL THAT APPLY)			
<input checked="" type="checkbox"/> Specification Number of pages [20]		Small Entity status is entitled to be, and hereby is, asserted for this application	
<input type="checkbox"/> Drawing(s) Number of sheets []		<input type="checkbox"/> Other (specify)	
METHOD OF PAYMENT (CHECK ONE)			
<input type="checkbox"/> A check in the amount of \$_____ is enclosed to cover the Provisional Filing Fee			
<input checked="" type="checkbox"/> The Commissioner is hereby authorized to charge filing fees of \$80.00 to Deposit Account Number 23-0804			

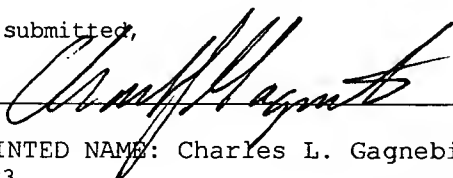
Please recognize the following attorneys with powers in this application.

Stanley M. Schurgin, Reg. No. 20,979
Charles L. Gagnebin III, Reg. No. 25,467
Victor B. Lebovici, Reg. No. 30,864
Beverly E. Hjorth, Reg. No. 32,033

Holliday C. Heine, Reg. No. 34,346
Gordon R. Moriarty, Reg. No. 38,973
James F. Thompson, Reg. No. 36,699
David A. Dagg, Reg. No. 37,809

Respectfully submitted,

SIGNATURE



DATE

11-21-03

TYPED or PRINTED NAME: Charles L. Gagnebin III
CLG/dkh/297783

REGISTRATION NO. 25,467

PROVISIONAL APPLICATION FILING ONLY

Express Mail No: EV 009947131 US

U.S. PROVISIONAL APPLICATION

ENTITLED

UNCOOLED CANTILEVER MICROBOLOMETER FOCAL PLANE ARRAYS
WITH mK TEMPERATURE RESOLUTIONS

BY

BIAO LI

XIN ZHANG

THOMAS BIFANO

ANDRE SHARON

EXPRESS MAIL NO: EV 009947131 US

INVENTION DESCRIPTION

A. General purpose of invention

Infrared (IR) detectors have extensive medical, industrial, military, and commercial applications. Broadly, they can be classified as either photonic detectors or thermal detectors. The minimum temperature resolution of IR cameras is characterized as noise equivalent temperature difference or NETD. Typically, a class of photonic detectors has fast response time and small NETD, but requires the devices to be kept at a reduced temperature (~ 80 K) to minimize the effects of internal thermal noise. The high cost of cryogenic IR cameras has limited their use to primarily scientific research and military applications.

By not necessitating a cooling system, IR cameras would require 20 times less power, be 10 to 100 times smaller in size, and cost 10 times less than cooled cameras. This invention relates to uncooled microbolometer infrared focal plane arrays (FPAs) with NETD in the mK range. A disruptive technology is proposed comprising double cantilever microbolometer focal plane arrays for uncooled infrared (IR) imaging.

B. Technical description of invention

B.1. Principle of cantilever bolometer arrays

The proposed invention will comprise a thermally sensitive bimaterial element that controls the position of two capacitor plates coupled to the input of a low noise MOS amplifier. A cross section of a pixel showing the major elements and materials of the double cantilever microbolometer structure is shown in Figure 1. The top and bottom plates of the sensing capacitor are composed of two overlapped free-standing bimaterial cantilevers. The orientation of the bimaterials for the top and bottom cantilevers is such that the metal layer on the bottom cantilever beam faces the metal layer on the top cantilever beam. The residual stress and curvature of each bimaterial layer will be modified by an ion implantation technique and/or varying layer thickness. An IR absorption layer will be deposited on the surfaces of both cantilevers.

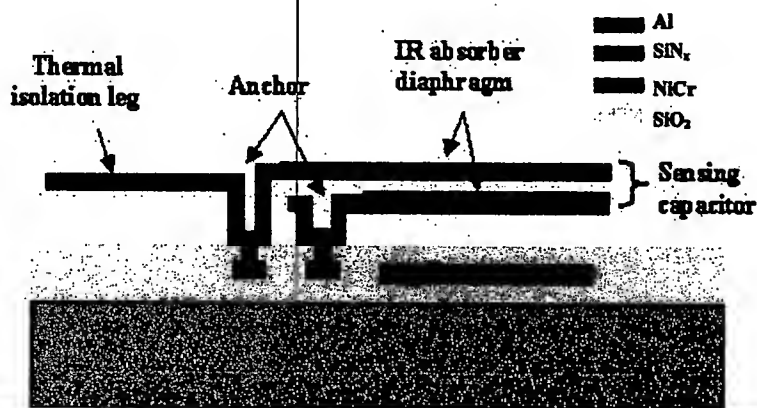


Figure 1: Cross section of a pixel showing the major elements and materials of the double cantilever microbolometer structure. The orientation of the bimaterials is such that the metal layer on the bottom cantilever beam faces the metal layer on the top cantilever beam.

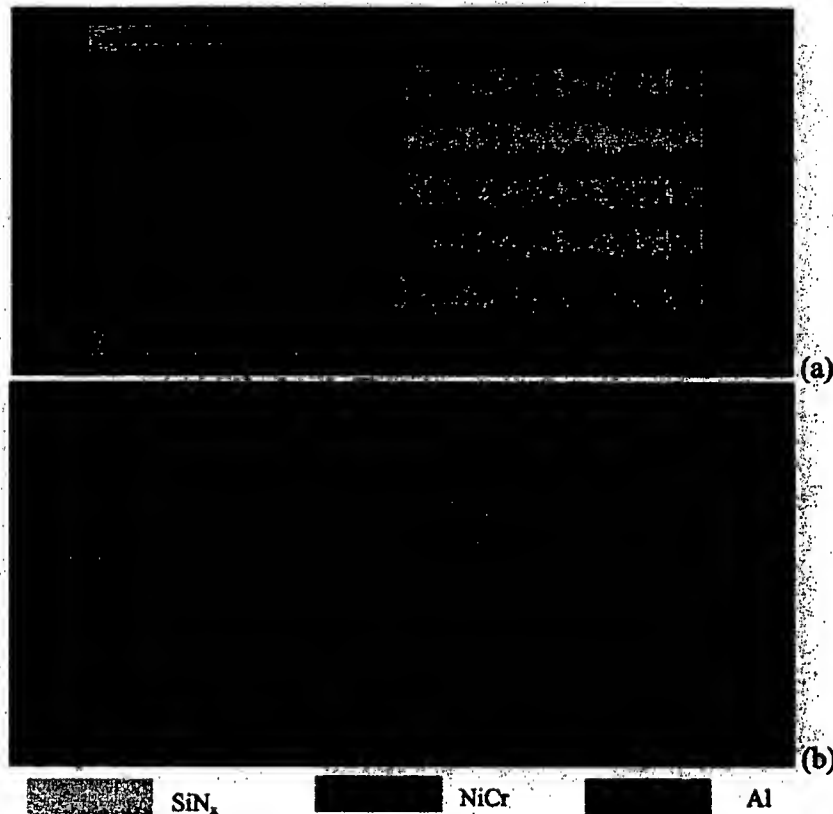


Figure 2: The exploded top view (a) and side view (b) of the double cantilever microbolometer structure. A thin IR absorber layer on the cantilever surfaces is not shown.

The bimaterial element with maximum difference in thermal-expansion coefficients would convert heat into mechanical movement. Since the metal layers on the top and bottom cantilever beams are designed to face each other, the IR irradiation would result in the top and bottom cantilevers deflecting in opposite directions, thus enabling a large change in the sensing capacitor. Figure 2 shows the finite element simulation of the double cantilever capacitor upon IR irradiation. As each layer flexes due to differential thermal expansion, it would control the position of individual capacitive plates coupled to the readout circuit. In our design, the thermally isolating support legs can prevent heat from being shunted down to the substrate, and the electrical connection on top of the thermal insulator is designed to have minimum impact on the thermal resistance.

B.2. Pixel design

When a microcantilever is exposed to infrared radiation, the temperature of the cantilever would increase due to absorption of the thermal energy. If two cantilevers are constructed from materials that exhibit dissimilar thermal expansion properties, these cantilevers would undergo bending due to differential surface stress in the structure. Assuming the width and thickness of each individual layer in bimaterials are identical, the deflection, z , at the free end of a cantilever introduced by thermal strain can be derived as,

$$z = \frac{k \cdot \Delta\alpha \cdot \Delta T \cdot L^2}{2t} \quad (1)$$

where k is a constant which is related to the material properties, $\Delta\alpha = \alpha_1 - \alpha_2$ is the difference of the thermal expansion coefficient for the bimaterials. L is the length, t the thickness of the individual layer, and ΔT the change in temperature. For a double cantilever structure, the sensitivity of the detection mechanism can be expressed as,

$$\bar{z} = |\Delta z / \Delta T|_{\text{top}} + |\Delta z / \Delta T|_{\text{bottom}} \quad (2)$$

where $|\Delta z / \Delta T|_{\text{top}}$ and $|\Delta z / \Delta T|_{\text{bottom}}$ represent the deflection per unit temperature for the top and bottom plates. The thermomechanical sensitivity of the sensing capacitor is given by,

$$S_T = \frac{\Delta C}{C_0} = \frac{\bar{z}}{z + z_0} \quad (3)$$

where z_0 is the initial gap distance of the sensing capacitor and \bar{z} is the average deflection.

In practice, the sensing structure, position of each element, and electronic addressing circuit may vary considerably. To optimize the design, the mechanical deflection of the cantilever microbolometer as a function of temperature change is simulated by a three-dimensional finite element program. Figure 3a shows the deformed structure of the double cantilever structure subjected to IR irradiation. Obviously, the top plate is bent up while the bottom one is bent down. The average movement of two plates relative to the change in temperature is $0.452 \mu\text{m/K}$. *NETD* for the double cantilever microbolometer is calculated as 8.6 mK . This value can be further reduced by decreasing the electrical noise from readout circuit. If the readout noise is negligible, *NETD* can be reduced to $\sim 2 \text{ mK}$.

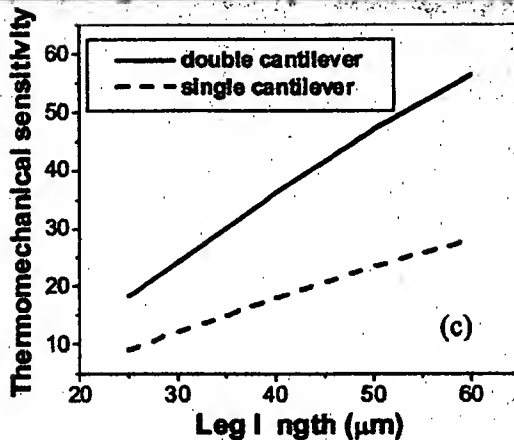


Figure 3: Finite element simulation of double and single cantilever microbolometer structures upon IR irradiation. (a) Double cantilever: $\bar{z} = 0.452 \mu\text{m/K}$, *NETD* = 8.6 mK . (b) Single cantilever: $\bar{z} = 0.227 \mu\text{m/K}$, *NETD* = 13 mK . (c) The calculated thermomechanical sensitivity of the double cantilever microbolometer is twice greater than the single cantilever microbolometer.

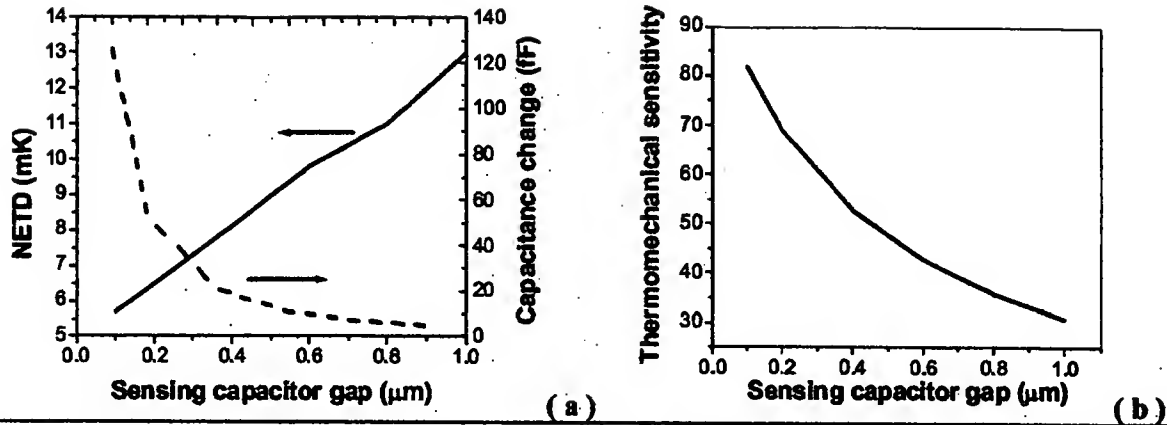


Figure 4: Effect of the sensing capacitor gap on (a) NETD and sensing capacitance, and (b) thermomechanical sensitivity for double cantilever microbolometer FPAs.

Figure 3b shows the finite element simulation of single cantilever microbolometer design. The temperature induced movement of the plate, $0.227 \mu\text{m/K}$, is half of the movement of the double cantilever structure. Correspondingly, its NETD value, 13 mK, is higher than that of the double cantilever microbolometer, 8.6 mK.

Figure 4 shows the effect of the sensing capacitor gap on NETD, sensing capacitance change and thermomechanical sensitivity for double cantilever microbolometer FPAs. All these parameters are benefited from the small gap distance. In the fabrication of the double cantilever microbolometer device, the sensing capacitor gap is controlled by the second sacrificial layer thickness.

B.3. Curvature modifications

As seen in Figure 4, the performance of cantilever microbolometer is affected significantly by the gap distance. Since the bimaterial cantilever structures are always curved due to the residual stress, it is of critical importance to manufacture the designed architecture with a flat curvature.

A neutral ion-machining technique has been developed in our team to alter the contour shape of free-standing thin-film structures by affecting their stress state. The ion beam can flat an initially curved microstructure by (i) rendering an amorphous thin film layer of material near the semiconductor surface, and (ii) removing material at the semiconductor surface after continuous bombardment. In a proof-of-concept experiment on MicroElectroMechanical Systems (MEMS) mirrors, we have demonstrated a nearly perfect planarity by using this technique; free-standing mirrors with radii curvature measured in meters were produced systematically. Another technique for curvature correction is varying the thickness of individual layers in bimaterial cantilever architectures. A finite element model has been built to characterize the effect of layer thickness on structure bending in double cantilever microbolometers.

C. Advantages and improvements over existing methods, devices or materials

Currently, two types of uncooled IR camera, i.e. resistive microbolometer and pyroelectric detector arrays, are commercialized. Both have demonstrated an NETD of less than 20 mK and 50 mK, respectively, and response time in the millisecond range. Further improvement of the performance of

these detectors, however, is limited by the fundamentals of the temperature coefficient of resistance (for resistive microbolometers) or the pyroelectric coefficient (for pyroelectric detectors), as well as high noise level.

Recent advances in MEMS have led to the development of uncooled single cantilever microbolometer arrays, which function based on the bending of a bimaterial beam upon absorption of optical energy. However, their manufacturability, planarity and reliability have been inadequate in systems. The released cantilever structures are always bent up due to the imbalance residual stress. In addition, the theory predicts that the sensitivity of the cantilever microbolometer is inversely proportional to the gap distance between the cantilever and the substrate. A small gap results in high performance. However, experimental results show that a small gap also leads to severe problems caused by stiction and sacrificial layer remaining in the released structure.

The advantages of the proposed double cantilever microbolometer FPAs include

- (i) Extremely high sensitivity. The temperature induced capacitance change of the double cantilever structure is about two times larger than that of the single cantilever structure. The NETD is about 13 mK and 8 mK for single and double cantilever microbolometers, respectively. Moreover, the double cantilever beams are flat rather than curved, and there is no any additional dielectric layer between two metal plates. This further increases the detection sensitivity.
- (ii) Low noise level. Since Johnson noise is negligible, the total noise of the cantilever microbolometer is about an order of magnitude lower than the resistive microbolometer.
- (iii) High image quality with pixel-by-pixel image-correction capability.
- (iv) Almost complete absorption of the IR irradiation. The incident IR light is absorbed by the overlapped top and bottom cantilevers that result in the sensing capacitance change. The resonant cavity with a $\lambda/4$ gap is designed to increase the IR absorption efficiency.
- (v) Flexibility in the design and fabrication. The thickness of the first sacrificial layer (between the substrate and the bottom cantilever) is $\sim 2.5 \mu\text{m}$ for the purpose of forming a $\lambda/4$ resonant cavity and releasing the structural bimaterial elements; whereas the thickness of the second sacrificial layer (between two cantilevers) is designed to be less than $0.5 \mu\text{m}$ for improving the sensitivity.
- (vi) Robust and IC foundry process compatibility. The reliability and fabrication yields are improved due to the simplified mechanical structure.

D. Possible variations and modifications

Currently, Al and SiN_x material pairs are used as the components of bimaterial cantilever beams. Other materials can be used to meet the requirement of efficient electrical conductance and/or infrared absorption.

An alternative design of the orientation of bimaterials is such that the semiconductor layer on the bottom cantilever beam faces the metal layer on the top cantilever beam (Figure 5). Such configuration is suitable for heavily curved cantilever beams. Without IR irradiation, the gap between bottom and top cantilever beams is not sensitive to residual stress induced bend.

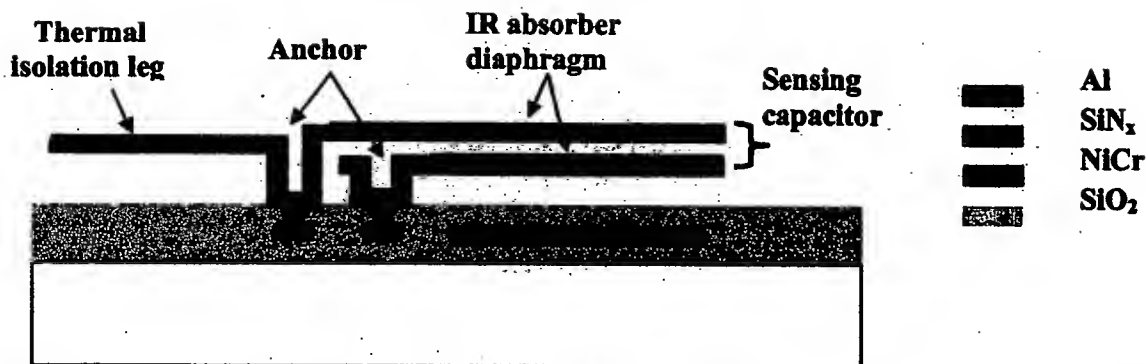


Figure 5: Schematic diagram of a double cantilever microbolometer. The orientation of bimetals is such that the semiconductor layer on the bottom cantilever beam faces the metal layer on the top cantilever beam.

E. Features believed to be new

The concept of cantilever microbolometer is different from the conventional pyroelectric or resistive microbolometer for uncooled IR detection. Bimaterial cantilever beams are adopted as the sensing elements which exhibit extremely high sensitivity and low noise. A robust, uncooled IR camera is expected to be fabricated whose performance is comparable with the best cryogenic IR detector (~5 mK temperature resolution).

F. Possible uses of invention

The uncooled microcantilever IR camera can be designed in different configurations to suit the specific need in future battlefield. Tanks have driving systems that rely on thermal IR imaging to navigate any terrain day or night. That is one of the benefits of thermal IR imaging technology, i.e. it can be used in daylight or complete darkness, totally independent of visible light. Ground forces can be issued small pocket sized thermal IR imagers for short to medium range surveillance and reconnaissance; whereas snipers can be furnished with thermal IR imaging weapon sights which can acquire and remove living targets from considerable distances.

G. State of development

The invention is used to develop a disruptive technology for the fabrication of robust, MEMS based double cantilever microbolometer arrays for uncooled infrared detection. The advantages of the pixel design include extremely high sensitivity and low noise. An ion beam machining technique is adopted to modify the residual stress and curvature of each bimaterial layer. Successful completion of the milestones proposed would lead to a flat double cantilever IR imaging system reaching a NETD in the mK range. Such uncooled microbolometer FPAs can compete with the best cryogenic ones (~5 mK NETD). The fabrication processing of such device is flexible and CMOS compatible.

H. Prospective commercial interest

The infrared camera has proved useful in a variety of applications. Law enforcement applications include criminal tracking, land/airborne surveillance, drug facility detection, or vehicles which have been

recently operated all from a safe distance; **industrial users** can detect flaws in manufacturing or weakened insulators, **fire safety professionals** can detect full vs. empty flammable storage containers, and **forestry workers** can easily track game or poachers. Other applications include non-destructive testing, process control, predictive and preventative maintenance, building and factory diagnostics, energy audits, roofing and insulation inspection, insurance fraud prevention, veterinary/human medical imaging, border patrol, remote security monitoring, and many more applications being discovered.

A two or three sentence, non-confidential description of its usefulness

The invention uses disruptive technology for the fabrication of an uncooled, flat cantilever microbolometer focal plane array whose performance is comparable with the best cryogenic IR detector. Such a device can be used for law enforcement, industry, fire safety professionals, forestry workers, and battlefield.

A one page non-confidential description of its usefulness

The infrared (IR) detectors described in this document have extensive medical, industrial, military, and commercial application. Broadly, they can be classified as either photonic detectors or thermal detectors. A class of photonic detectors has fast response time and small NETD (noise equivalent temperature difference), but requires the devices to operate at very low temperatures (~80 K) to minimize the effects of thermal induced noise. The high cost of these cryogenic IR cameras has limited their use primarily to scientific research and specialized military applications.

By eliminating the requirement for cryogenic cooling, IR cameras would require 20 times less power, be 10 to 100 times smaller in size, and cost 10 times less than cooled cameras. Currently, two types of uncooled IR cameras (i.e. resistive microbolometer and pyroelectric detector arrays) are available commercially. Both have demonstrated an NETD of less than 20 mK and 50 mK, respectively, and response times in the millisecond range. However, further improvement to the performance of these detectors is limited by the fundamentals of the temperature coefficient of resistance (for resistive microbolometers) or the pyroelectric coefficient (for pyroelectric detectors), as well as high noise level associated with this design.

The invention employs a disruptive technology for the fabrication of a robust, MicroElectroMechanical System (MEMS) based microbolometer array for uncooled infrared detection. The advantages of this pixel design include extremely high sensitivity and low noise. Such uncooled microbolometer infrared focal plane arrays (FPAs) have similar or better sensitivity than cryogenic based sensors (~5 mK NETD) and the fabrication/processing of such a device is flexible and CMOS compatible.

An uncooled microcantilever IR camera can also be designed in different configurations to suit the specific need. **Law enforcement** applications include criminal tracking, land/airborne surveillance, and drug facility detection, all from a safe distance. **Industrial users** can use the device to detect flaws in manufacturing or damaged insulators. **Fire safety professionals** can detect full vs. empty flammable storage containers. **Forestry workers** can easily monitor the movement of animals or identify illegal hunting. In the future battlefield, ground forces can be issued **small pocket sized thermal IR imagers** for short to medium range surveillance and reconnaissance; whereas snipers can be furnished with **thermal IR imaging weapon sights** which can acquire thermal radiant targets from considerable distances. Other applications include non-destructive testing, process control, predictive and preventative maintenance, building and factory diagnostics, energy audits, roofing and insulation inspection, veterinary/human medical imaging, border patrol, remote security monitoring, and many more applications yet to be discovered.

Optical and Infrared Detection Using Microcantilevers

P. I. Oden, E. A. Wachter, T. Thundat and R. J. Warmack

Oak Ridge National Laboratory, P.O. Box 2008, Oak Ridge, Tennessee, 37831-6123

P. G. Datskos

Consultec Scientific, Inc., 725 Pellissippi Parkway, Knoxville, Tennessee, 37932-3300

ABSTRACT

The feasibility of micromechanical optical and infrared (IR) detection using microcantilevers is demonstrated. Microcantilevers provide a simple means for developing single- and multi-element sensors for visible and infrared radiation that are smaller, more sensitive and lower in cost than quantum or thermal detectors. Microcantilevers coated with a heat absorbing layer undergo bending due to the differential stress originating from the bimetallic effect. Bending is proportional to the amount of heat absorbed and can be detected using optical or electrical methods such as resistance changes in piezoresistive cantilevers. The microcantilever sensors exhibit two distinct thermal responses: a fast one ($\tau_1^{\text{thermal}} < ms$) and a slower one ($\tau_2^{\text{thermal}} \sim 10ms$). A noise equivalent temperature difference, NEDT = 90 mK was measured. When uncoated microcantilevers were irradiated by a low-power diode laser ($\lambda = 786 nm$) the noise equivalent power, NEP, was found to be $3.5nW/\sqrt{Hz}$ which corresponds to a specific detectivity, D^* , of $3.6 \times 10^7 cm \cdot \sqrt{Hz}/W$ at a modulation frequency of 20 Hz.

2. INTRODUCTION

Because infrared is the second most intense radiation band in our environment, its detection and imaging has extensive industrial, military, and commercial applications, including remote monitoring of facilities and equipment, process control, surveillance, night-vision, collision avoidance, and medical imaging. Presently, there are several families of commercially available infrared detectors, including thermopiles, pyroelectrics, bolometers, and various solid state detectors^{1,2}. Thermopile detectors typically have a large thermal mass and long response times ($> 10ms$). Bolometers using micromachined, suspended foils have much better rise times due to their reduced mass. Both thermopiles and bolometers offer broad spectral response when coated with suitable optically absorbing materials. Solid state detectors for the infrared region, such as quantum well devices, must generally be operated at reduced temperatures due to inherently high thermal noise. Additionally, the spectral response of these semiconductor devices is limited by the intrinsic properties of the composing materials. These infrared detectors can be classified either as quantum - such as the pyroelectrics; or thermal detectors - such as bolometers and thermopiles. For the former type, incident infrared radiation is converted into an electronic response while with thermal detectors, IR radiation is converted into heat which is subsequently detected through temperature changes in the detector. Depending on the operational demands, one type of detection device may be favored over another. As a general rule, when the photon energy of the infrared radiation $h\nu > k_B T$, photon detectors offer better performance and when $h\nu < k_B T$, thermal detectors are generally favored.

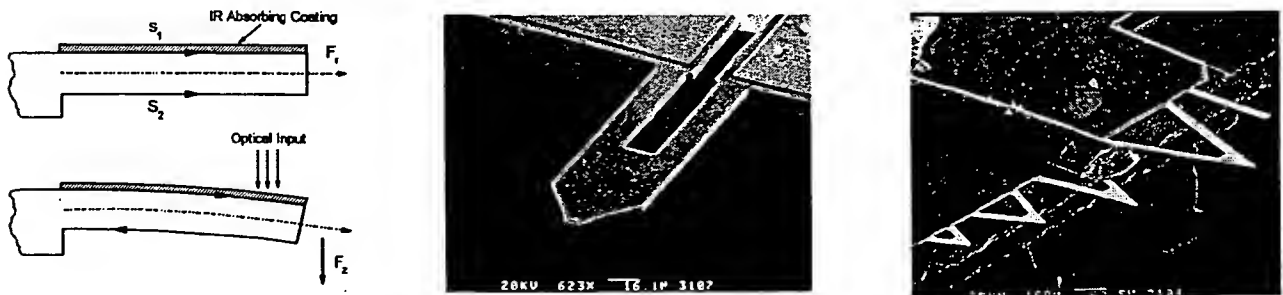


Figure 1. Left drawing is a cross-sectional schematic showing the bending response of a bimetallic cantilever with an IR adsorbing coating. Surface stresses S_1 and S_2 are balanced at equilibrium, generating a radial force F_r along the medial plane of the microcantilever. These stresses become unequal upon exposure to IR radiation producing a bending force, F_z , that displaces the tip of the microcantilever. Middle - is a scanning electron micrograph of one of the piezoelectric IR sensors used (calibration bar is $16\mu m$). Right - is another scanning electron micrograph of the Si_3N_4 microcantilevers used for the experiments compared to a human hair (calibration bar is $62.5\mu m$).

A new approach for producing compact, light-weight, highly-sensitive micromechanical infrared detectors is provided by microcantilever technology which is based on the bending of a microcantilever resulting from absorption of optical energy. When a microcantilever is exposed to infrared radiation, the temperature of the cantilever increases due to absorption of this optical energy^{3,4}. If these microcantilevers are constructed from materials exhibiting dissimilar thermal expansion properties (such as silicon nitride coated with a thin gold film), the bimetallic effect will cause the microcantilever to bend in response to this temperature variation³⁻¹⁴ (such a response is shown in the left image of Figure 1). The extent of bending is directly proportional, in first order, to the rate of energy absorption, which in turn is proportional to the radiation intensity. Previous work has shown that microcantilever bending can be detected with extremely high sensitivity¹⁵⁻¹⁷. For example, the metal-coated microcantilevers that are commonly employed in atomic force microscopy (AFM) allow sub-Angstrom ($<10^{-10}m$) sensitivity to be routinely obtained. Recent studies have reported^{9,14} the use of microcantilever bending for calorimetric detection of chemical reactions with energies as low as a few pJ . It was demonstrated³ that the detector had an observed sensitivity of $100 pW$ corresponding to an energy of $150 fJ$ and proposed using the sensor as a femtojoule calorimeter. An estimate of the minimum detectable power level was of the order of $10 pW$, corresponding to a detectable energy of $20 fJ$ and a temperature sensitivity $10^{-5} K^9$. However, using an optimally designed cantilever, the sensitivity may be improved even further¹⁰⁻¹³. Hence, for applications in optical radiation detection, microcantilevers can be coated with appropriate absorptive materials such that they undergo bending upon exposure to radiation (such as infrared or near infrared radiation). IR sensing cantilevers are typically $100 - 200 \mu m$ long, $0.3 - 4 \mu m$ thick and $10 - 50 \mu m$ wide, and made out of materials such as silicon nitride, silicon or other types of semiconducting materials¹⁸. Due to the monolithic nature of these devices, they can easily be produced in one- and two-dimensional arrays with hundreds of levers on a single wafer. This type of fabrication scheme possesses obvious advantages when considering the production of infrared imaging systems with these cantilever devices.

When considering the bending of the lever, a proportionality between bending and the absorbed energy by the microcantilever is obtained by assuming a spatially uniform incident power, dQ/dt , onto a bimetallic microcantilever. Therefore, the maximum deflection, z_{max} , due to differential stress is given by^{3,11,13,19}:

$$z_{max} = \frac{5}{4} \frac{(t_1 + t_2)l^3}{(\lambda_1 t_1 + \lambda_2 t_2)wt_2^2} \cdot \frac{\eta(\alpha_1 - \alpha_2)(dQ/dt)}{4(1 + t_1^2/t_2^2) + 1/t_1 t_2 (6t_1^2 + E_1 t_2^2/E_2) + E_1 t_1^3/E_2 t_2^3} \quad (1)$$

where l and w are, the length and width of the microcantilever, respectively, t_1 and t_2 are the thicknesses of the two layers, λ_1, λ_2 ; α_1, α_2 ; E_1, E_2 are the thermal conductivities; thermal expansion coefficients and Young's moduli of elasticity of the two layers; η is the fraction of the radiation power absorbed.

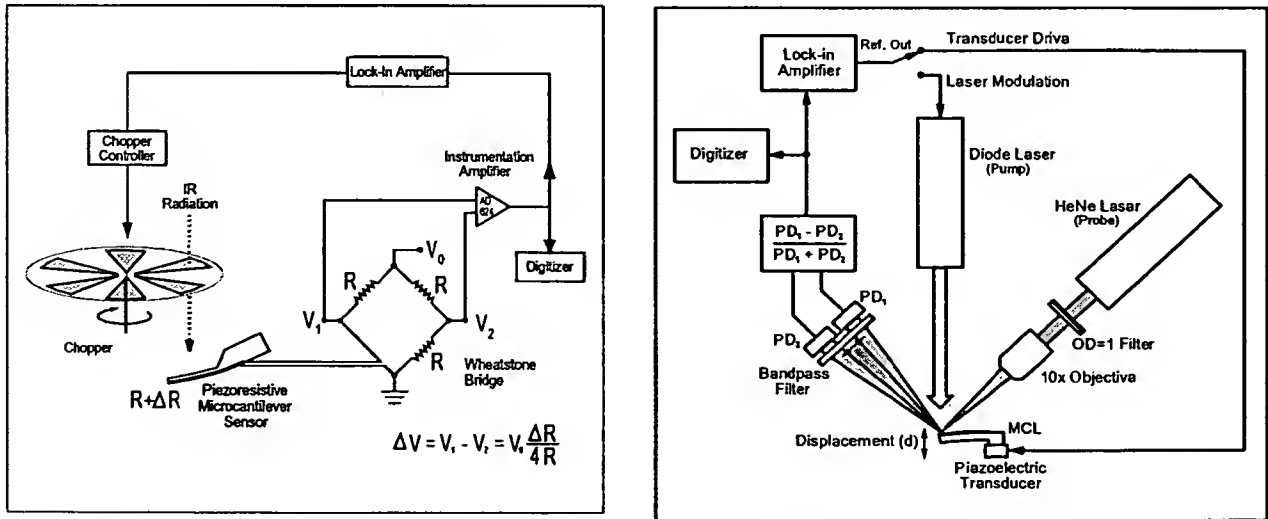


Figure 2. (a) Schematic representation of the piezoresistive IR detection experiment. The piezolever is part of a Wheatstone bridge, one of the legs connected to ground, the other to a metal film resistor with approximately the same resistance $R \sim 2000 \Omega$. The other two outputs are connected to the input of a differential instrumentation amplifier. (b) Schematic diagram of the optical read-out method for IR detection.

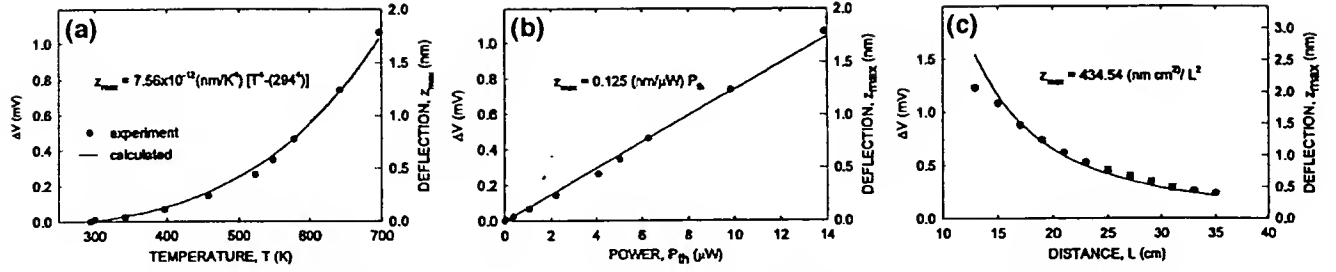


Figure 3. (a) Response of the Wheatstone bridge detection circuit, ΔV , and deflection, z_{\max} , of the piezolever as a function of the source temperature. (b) Response as a function of the absorbed thermal power and (c) as a function of IR source distance, L .

3. EXPERIMENTAL

3.1. Piezoresistive Deflection Monitoring

A schematic diagram of the piezoresistive cantilever deflection detection technique is given in Figure 2(a). In this example, surface doped silicon microcantilevers were used in which the piezoresistance across the cantilever varied when it bent due to thermal stimulation. The design and construction of these cantilevers is described in detail elsewhere^{20,21}. The total resistance of the cantilever was approximately 2000Ω , which was electrically connected across one arm of a dc-biased Wheatstone bridge circuit. The change in the total resistance is directly proportional to the maximum deflection of the cantilever²⁰:

$$\Delta R(T) = 3 R z_{\max}(T) \times 10^{-6} \quad (2)$$

where $z_{\max}(T)$ is expressed in nm.

The thermally induced deflection of the cantilever is caused by the bimetallic effect which arises due to the difference in the thermal properties of the IR coating, the metal layer, and the native silicon body of the cantilever. A reference voltage V_0 (equal to 9 volts in these experiments) was applied across the circuit and the voltage difference, $\Delta V(T)$, across the Wheatstone bridge circuit was digitized using a Tektronix TDS 544A digital oscilloscope or fed into a Stanford Research Systems SR850 lock-in amplifier. The measured voltage ΔV is related to the deflection of the cantilever by

$$\Delta V(T) = \frac{3V_0}{4} z_{\max}(T) \times 10^6 \quad (3)$$

The experimental measurements were performed using piezoresistive microcantilevers as temperature sensors in the configuration shown in Figure 2(a). The commercially available piezolever¹⁸ was coated with $\sim 50 \text{ nm}$ of gold black which served as the IR absorbing material. IR radiation was then focused onto the sensor using a 2.54 cm diameter IR lens with a focal length of 3.5 cm and a wavelength transmission range between $0.6\text{--}15 \mu\text{m}$ ²². A Stanford Research Systems SR-540 chopper was used to modulate the IR radiation upon the detector. The sensor assembly was positioned 15 cm from a soldering iron which served as the IR source. A calibrated thermocouple was attached to the IR source so that its temperature could be recorded.

The thermal power absorbed by the detector can be described as:

$$P_{\text{thermal}} = \eta \frac{dQ}{dt} = \eta t_L \left(\frac{A_D}{2\pi L^2} \right) A_S \epsilon \sigma_{S-B} (T_S^4 - T_R^4) \quad (4)$$

where t_L is the transmission of the lens, A_D is the effective area of the sensor, L is the distance of the detector from the source, A_S is the area of the target (IR source), ϵ is the target's emissivity, σ_{S-B} is the Stefan-Boltzmann constant ($\sim 5.67 \times 10^{-12} \text{ W} \cdot \text{cm}^{-2} \cdot \text{K}^{-4}$), T_S is the temperature of the target, and T_R is the background temperature. In the present

studies $t_L \sim 0.7$, $A_D = 6.2 \times 10^{-4} \text{ cm}^2$, $L \sim 15 \text{ cm}$, $A_S \sim 90 \text{ cm}^2$, and $T_R = 294 \text{ K}$. Using these values in Eq. (4), the absorbed thermal power (in Watts) is $P_{\text{thermal}} \sim 6.064 \times 10^{-17} [T_S^4 - (294)^4]$ (assuming that $\eta \sim 0.9$ and a measured $\epsilon \sim 0.43$ for the hot iron IR source).

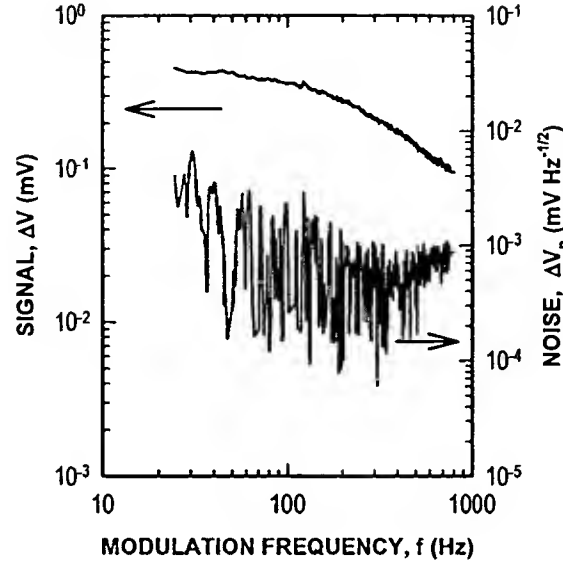


Figure 4. Response of the Wheatstone bridge detection circuit, ΔV , deflection, z_{max} and noise ΔV_n of the piezolever as a function of the modulation frequency.

The response ΔV was measured as a function of the temperature, T , of the IR source. This is plotted in Figure 3(a) along with the deflection, z_{max} , of the piezolever and can be seen to be a monotonically increasing function of temperature. In Figure 3(b) a plot of the response of Wheatstone bridge circuit, ΔV , and the deflection, z_{max} , of the piezolever detector as a function of the total power absorbed by the detector and it can be seen that it increases linearly with increasing power. From the slope of this line, a deflection sensitivity of $0.125 \text{ nm} / \mu\text{W}$ is obtained. At a modulation frequency of 30 Hz , a noise equivalent power (NEP) of $\sim 70 \text{ nW} / \text{Hz}^{1/2}$ was also obtained, where $\text{NEP} = (\Delta V_n / \Delta V) \times P_{\text{thermal}}$; ΔV_n is the background noise level ($\Delta V_n \sim 10^{-6} \text{ V}$).

The response of the detector was also measured as a function of the distance from an IR source. This is shown in Figure 3(c) where ΔV and z_{max} are plotted as a function of the distance, L , between the detector and the surface of the soldering iron (IR source); L was varied from 14 cm to 35 cm . The ambient temperature was $\sim 294 \text{ K}$ and the temperature of the IR source was held at 693 K . The measured ΔV and calculated z_{max} were found to decrease with increasing distance and followed closely an inverse square relationship with distance [see Eq. (4)] for distances larger than 15 cm .

Since the response of any thermal sensor depends on both the amount of heat falling onto the detector and the length of time it is exposed to the incoming IR radiation we measured the response of the Wheatstone bridge circuit, ΔV , and the deflection, z_{max} , as a function of modulation frequency of the IR radiation (Figure 4). It can be seen that the detector response (and the deflection of the cantilever) decreases with increasing modulation frequency. The temporal response of the temperature sensor was also determined by measuring ΔV as a function of time. The microcantilever was found to exhibit two thermal response times due to the incoming IR radiation; a time $\tau_1^{\text{thermal}} < 1 \text{ ms}$ and a time τ_2^{thermal} that is somewhat longer ($\sim 10 \text{ ms}$).

These findings demonstrate that small changes in temperature induce deflections of the microcantilever correspond to measurable changes in the piezocantilever resistance. It should be noted that these commercially available piezolevers have been designed to be minimally sensitive to changes in temperature so as to reduce the noise and interference in scanning probe microscopy applications. Therefore, the temperature sensitivity of the piezolever could be further improved by optimizing its shape, IR absorbing coating and thermal isolation.

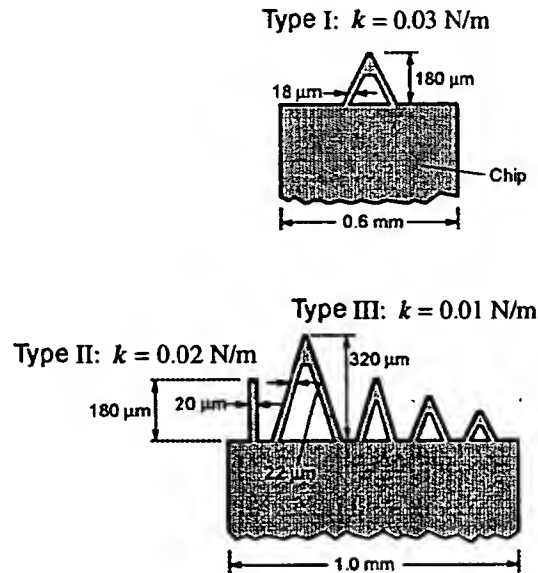


Figure 5. Schematic view of the $0.6 \mu\text{m}$ thick Si_3N_4 microcantilevers used for evaluation of thermal response. Note that results from only the two left-most microcantilevers (out of five total) on the lower chip are presented.

3.2. Optical Deflection Monitoring

Bending of microcantilevers can readily be determined by a number of means, including optical, capacitive, tunneling, and, as shown before, piezoresistive. The optical deflection approach used was adapted from standard atomic force microscopy imaging systems, and is shown in Figure 2(b). Microcantilevers were mounted in a holder (from Digital Instruments) designed for tapping mode AFM, which secured the base of the microcantilever against a small piezoelectric transducer; this chip holder was then mounted on a three-axis translation stage to facilitate fine adjustment of the microcantilever relative to the rest of the experimental apparatus. Collimated optical radiation from a diode laser was used to evenly illuminate the mounted microcantilever (pump wavelength of 786 nm , beam diameter of 6 mm , centered on the tip of cantilevers $180 - 320 \mu\text{m}$ in length). Output of this excitation source was modulated sinusoidally at frequencies ranging from DC to 100 kHz , with peak powers ranging from 0 to 18.5 mW (0 to 65 mW/cm^2). This configuration provided a flexible, easily controlled test system for quantifying microcantilever response to optical energy. All measurements were conducted at ambient temperature and atmospheric conditions.

A second laser was used in a probe configuration to monitor bending. A helium-neon laser (or HeNe, delivering 3 mW at 633 nm) was focused onto the tip of the microcantilever using a $10\times$ microscope objective; to minimize heating of the tip by the probe laser, optical power was reduced by placing a neutral density filter with an optical density of 1.0 between the probe laser and the objective. A dual element photodiode displacement detector was used to collect the reflected probe beam [position detectors PD_1 and PD_2 in Figure 2(b)]; a 1 nm bandpass filter centered at 633 nm was placed in front of the detector to block scattered light from the pump laser. The difference signal from the detector pair as the cantilever tip changed position $\left(\frac{PD_1 - PD_2}{PD_1 + PD_2} \right)$ was used to measure the displacement, d . This signal was directly digitized and stored, or sent to a lock-in amplifier (SR850, Stanford Research Systems) for signal extraction and averaging. The lock-in amplifier was also used to control modulation frequency and output level of the pump laser.

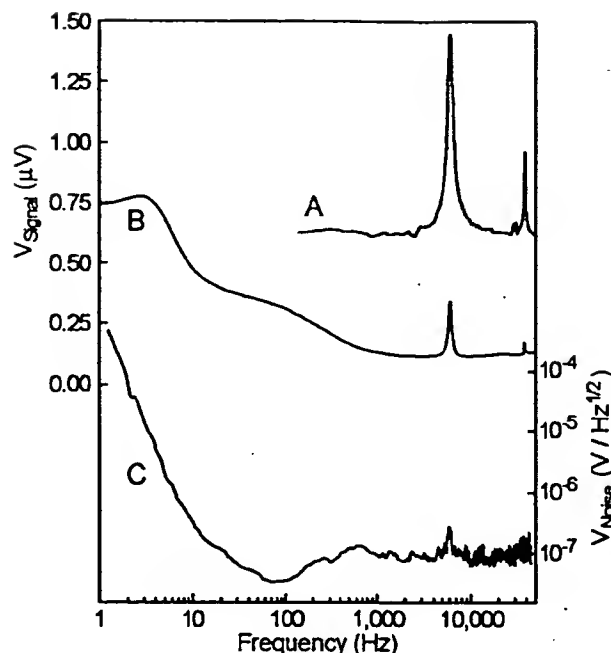


Figure 6. Mechanical and optical excitation spectra for a Type III microcantilever. Response to frequency swept mechanical excitation is given in spectrum 'A'; similar results for optical excitation are shown in spectrum 'B'. Optical excitation was effected using a sinusoidally modulated pump laser at 786 nm . Spectrum 'C' shows noise response when the pump laser is operated in a dc mode. Fundamental mechanical resonance at 6.2 kHz and higher-order resonance at 37 kHz are evident for both optical and mechanical excitation.

Optical response characteristics of three different types of commercially available AFM probe tips were evaluated. These microcantilevers are shown schematically in Figure 5 as well as in the scanning electron micrograph of Figure 1. Microcantilevers typically come from the manufacturer attached to a large rectangular chip (ca. 1 mm wide x 3 mm long x 1 mm thick) that is used to facilitate manipulation and mounting, and all those evaluated in this work were used as received. The microcantilevers used were: a triangular silicon nitride Si_3N_4 microcantilever (labeled "I" in Figure 5, with a length of $180\text{ }\mu\text{m}$, a width of $18\text{ }\mu\text{m}$ and a bending force constant $k \sim 0.3\text{ N/m}$, from Park Scientific); a rectangular silicon nitride microcantilever (labeled "II", $200\text{ }\mu\text{m}$ in length and $20\text{ }\mu\text{m}$ in width, bending force constant $k \sim 0.2\text{ N/m}$, Park Scientific); and a triangular silicon nitride cantilever (labeled "III", which was $320\text{ }\mu\text{m}$ long and $22\text{ }\mu\text{m}$ wide, with a bending force constant $k \sim 0.1\text{ N/m}$, Park Scientific). Each was $0.6\text{ }\mu\text{m}$ thick. The Type I cantilever was coated with aluminum on one side to see how this would affect its optical response characteristics; Types II and III were used as received from the manufacturer, with a gold/chromium film uniformly covering one side.

An essential aspect of any scheme for micromechanical optical detection is the ability to sensitively detect physical changes resulting from thermal stress, since this directly affects the sensitivity and precision in measurement of temperature change or thermal flux. As an initial evaluation of the ability to detect optically-induced bending of a microcantilever, each of the three types of microcantilever were subjected to both mechanical and optical excitation, and their response measured as a function of excitation frequency. Mechanical excitation was achieved by driving the piezoelectric element in the AFM chip holder with the reference signal from the lock-in amplifier; such mechanical excitation spectra are helpful in locating resonance frequencies for allowed microcantilever bending modes. Optical excitation spectra were obtained by modulating the pump laser with the lock-in reference signal. Typical response spectra for a triangular microcantilever (Type III) are shown in Figure 6. The mechanical spectrum (curve "A") shows two resonances, at 6 kHz and 38 kHz , attributable to the fundamental transverse resonance and a higher-order resonance (possibly torsional bending), respectively. The optical spectrum (curve "B") shows similar resonance features, although with somewhat different relative intensities; a large, broadband response is also noted at low frequencies. No synchronous oscillatory response was noted when the microcantilever was excited with constant dc laser power (curve "C"). Similar response was noted under these conditions for the other two microcantilevers.

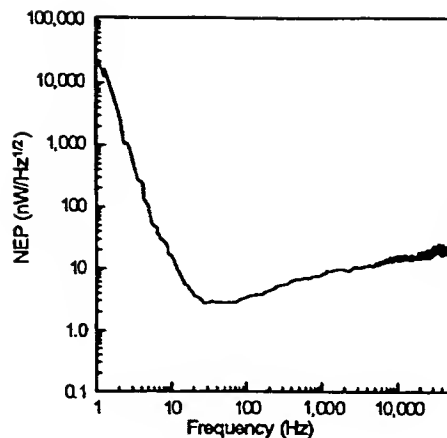


Figure 7. Noise equivalent power (NEP) as a function of modulation frequency for a Type III Si_3N_4 microcantilever. Optical excitation at 785 nm , utilizing bimetallic bending induced in a gold/chromium film.

Figure 6(B) shows that microcantilever response to optical input decreases rapidly for frequencies above 10 Hz , but that mechanical resonance is still observed even at frequencies well above 10 kHz . In fact, the Type I and II microcantilevers exhibited strong optical resonance at frequencies of 17 kHz and 14 kHz , respectively; these modes correspond to the fundamental transverse resonances for the microcantilevers. Such resonant response demonstrates that reversible heating and bending of the cantilever occurs as a result of optical excitation, producing mechanical vibration. These resonances also have quality factors that are identical to their mechanically-driven counterparts, confirming that optically-pumped mechanical vibration is occurring.

The rapid roll-off in response observed in Figure 6(B) is attributed to thermal equilibration of the cantilever at high modulation frequencies. Because the cantilever must dissipate heat between laser pulses, the finite thermal conductivity of its legs limits the rate at which heat from these thermal impulses can be transferred out of the microcantilever and into the support structure (the chip); thus, as modulation frequency is increased and the microcantilever approaches thermal equilibrium, changes in thermal stress as a function of time approach zero. Comparison of the response of the Type II and Type III cantilevers showed that the rectangular Type II microcantilever had a higher relative response at frequencies above 7.5 kHz . We believe this is due to more effective thermal transfer for the rectangular geometry. Since the rectangular microcantilever does not have a geometric restriction between the cantilever and the chip, transfer of thermal energy absorbed at the tip should be more rapid than that for the triangular microcantilever, which has a large area tip suspended on relatively narrow legs. The direct route of thermal transfer in the rectangular microcantilever appears to allow it to maintain a thermal differential at higher optical modulation frequencies, and hence to continue responding to the time varying optical stimulus at frequencies well above those practical with the triangular geometry.

In order to evaluate the role of optical reflectivity (or thermal absorptivity) on microcantilever response, a silicon nitride microcantilever (the Type I specimen) was coated on one side with a thin layer of aluminum; note that the manufacturer's gold/chromium film was removed prior to aluminum deposition. This produced a microcantilever that had a nearly transparent body that was highly reflective to the pump laser on the aluminum coated side (reflectivity, $R \sim 0.95$ at 786 nm), but slightly less reflective on the uncoated side (due to absorption of the pump radiation upon transmission through the Si_3N_4 cantilever body). As expected, the resonant frequency of this cantilever was found to be 17 kHz . However, when the uncoated side of the microcantilever was illuminated (reverse geometry), the magnitude of bending response at all frequencies increased by about 20% in comparison to normal illumination on the reflective side. We believe this difference is attributable to increased absorption of the pump beam upon transmission through the Si_3N_4 material, resulting in more effective transduction of optical energy into thermal heating of the microcantilever. While this simple experiment demonstrates that sensitivity can be improved by increasing absorption of impinging optical radiation, it is obvious that to optimize the method further suitable optically absorbing coatings are needed (such as carbon black, gold black, or other broadband absorbers). Unfortunately, such materials were not available for this study.

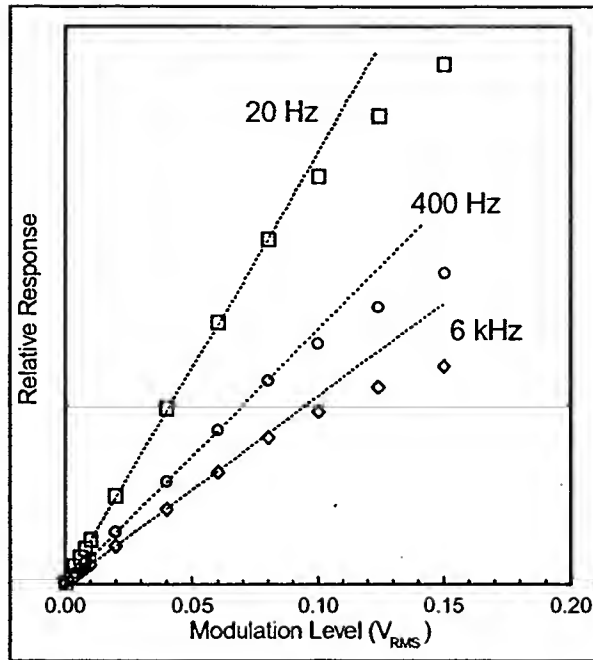


Figure 8. Photometric response for a typical microcantilever (Type III) at various optical pump levels using excitation at 20Hz, 400Hz and 6kHz.

Photometric response was further characterized by measuring microcantilever response at various modulation frequencies and optical pump levels (Figures 6 and 7, and Table I). For the Type III Si_3N_4 microcantilever, we estimate a noise equivalent power (NEP) of 3.5 nW/Hz at 20Hz, where $\text{NEP} = (V_{\text{noise}}/B)(P/V_{\text{signal}})$, V_{noise} is the background noise level on the cantilever over a lock-in amplifier bandwidth, B , of 0.26 Hz , and P is the incident optical power producing an observed signal, V_{signal} . Specific detectivity, D^* , is equal to $3.6 \times 10^7 \text{ cm} \cdot \text{Hz}^{1/2}/\text{W}$ under these conditions, where $D^* = (A^{1/2} V_{\text{signal}})/(V_{\text{noise}} P)$, and A is the area of the detector element. Note that the characteristics of this initial, unoptimized microcantilever compare quite favorably with some room temperature technologies currently under development, including indium antimonide photoconductors ($\text{NEP} = 5 \text{ nW}$ at 500 Hz)²³, but are not yet competitive with silicon microbolometers ($\text{NEP} = 5 \text{ pW/Hz}$, $\text{NETD} = 40 \text{ mK}$ at 30 Hz)²⁴ or pyroelectric devices ($\text{NEP} = 8 \text{ pW/Hz}$, $D^* = 3.5 \times 10^8 \text{ cm} \cdot \text{Hz}^{1/2}/\text{W}$)²⁵. However, in contrast to these highly optimized examples, several simple improvements to our microcantilever system are obvious that could improve performance dramatically. For instance, since the metal coating on

Table I. Photometric response at 785nm for a gold/chromium coated Si_3N_4 microcantilever (Type III). Data at 6.02kHz was obtained at the mechanical of the microcantilever.

Optical Modulation Frequency (Hz)	Detector Time Constant (ms)	V_{signal} (μV)	V_{noise} (μV)	NEP (nW/Hz)	D^* ($\text{cm} \cdot \text{Hz}^{1/2}/\text{W}$)
6020	300	307.1	0.585	13.1	9.48×10^6
	30	305.3	1.76	12.5	9.91×10^6
	1	305.5	9.46	12.3	1.01×10^7
400	300	223.2	0.196	6.03	2.06×10^7
	30	221.1	0.691	6.78	1.83×10^7
	10	226.3	1.19	6.59	1.88×10^7
20	300	528.2	0.266	3.46	3.59×10^7

the tested cantilevers is highly reflective at the pump wavelength (for gold, $R > 98\%$ at 785 nm), use of an improved absorptive coating (such as gold black, $R < 2\%$) could improve NEP in this example to $< 75\text{ pW}$. Furthermore, the observed detection limits appear to be determined by readout noise in our optical detection circuit. We believe that with careful design of this circuitry, performance could be substantially improved. Finally, response of the microcantilevers was extremely linear (with a correlation coefficients, $r_2 > 0.99995$) for all but the highest test levels; roll-off in measured response for very high laser modulation levels is an artifact of our method for modulating the pump laser, which exhibited a reduced depth of modulation at high drive levels.

4. CONCLUSIONS

We have demonstrated that microcantilevers represent an important development in room temperature infrared detector technology, and can be expected to provide the basis for considerable further development. For example, while the microcantilevers employed here were optimized for standard AFM applications (and were in fact designed to minimize thermal sensitivity), vastly improved detectors could be produced by making relatively simple changes in the materials and geometries used in microcantilever fabrication. It is possible to design microcantilevers with much smaller force constants by varying the geometry of the cantilever, and in contrast to the devices used in this study, cantilevers with force constants as small as 0.006 N/m are now commercially available. Since the fundamental mechanical resonance frequency of a microcantilever is proportional to \sqrt{k} , reductions in force constant can be used to bring resonance into ranges compatible with mechanical chopping frequencies. It is also clear that the coatings applied to the cantilever are at least as important as the composition of the cantilever itself. For example, high thermal expansion bimetallic coatings (such as films of Al, Zn, Pb, or In) could be used to increase the thermally-induced bending of the cantilever. Coating the surface of the cantilever with high emissivity materials (such as gold black) can also enhance IR response.

Since microcantilever spectral response can be easily tailored through the application of specific absorptive coatings, choice of material for fabrication of the microcantilever can be determined primarily by the requirements of the manufacturing process. This means that microcantilevers can be fabricated using standard semiconductor methods and materials, and as a consequence could be mass produced at very low cost. Hence, two-dimensional cantilever arrays based on the technology described here could become very competitive with existing technologies due to their inherent simplicity, high sensitivity, and rapid response to optical radiation. While the optical readout method is useful with single element designs, practical implementation of microcantilever arrays may require the use of other readout methods, such as piezoresistance. Fortunately, the microcantilever technology's compatibility with a variety of readout methods also affords tremendous flexibility to potential system designers.

5. ACKNOWLEDGEMENTS

Research sponsored by U.S. Department of Energy under contract DE-AC05-96OR22464 with Lockheed Martin Energy Research Corp. The authors wish to acknowledge the support of the ORNL Seed Money Program. The efforts of P.I. Oden were supported, in part, by an appointment to the Alexander Hollaender Distinguished Postdoctoral Fellowship Program sponsored by the U.S. Department of Energy, Office of Health and Environmental Research, and administered by the Oak Ridge Institute for Science and Education. P.G. Datskos wishes to acknowledge the support of the National Science Foundation under the SBIR award DM2-9460929 to Consultec Scientific, Inc.

6. REFERENCES

1. R. J. Kayes, Editor "Optical and Infrared Detectors," *Topics in Applied Physics*, Volume 19, Springer Verlag Berlin (1977).
2. P. Howard, J. Stevens, C. Rau, R.J. Herrring, and R.A. Wood, *Infrared Technology XXI*, SPIE Vol. 2552-60, July 1995.
3. J.R. Barnes, R.J. Stephenson, C.N. Woodburn, and M.E. Welland, *Rev. Sci. Instrum.*, **65**, 3793 (1994).
4. O. Nakabeppu, M. Chandrachood, Y. Wu, J. Lia, and A. Majumdar, *Appl. Phys. Lett.*, **66**, 694 (1995).
5. N. Umeda, S. Ishizaki, and H. Uwai, *J. Vac. Sci. Technol.*, **B9**, 1318 (1991).

6. M. Allegrini, C. Astoli, P. Baschieri, F. Dinneli, C. Frediani, A. Lio, and T. Mariani, *Ultramicroscopy*, **42-44**, 371 (1992).
7. O. Marti, A. Ruf, M. Hipp, B. Bielefeldt, J. Colchero, and J. Mlynek, *Ultramicroscopy*, **42-44**, 345 (1992).
8. J. Mertz, O. Marti, and J. Mlynek, *Appl. Phys. Lett.*, **62**, 2344 (1993).
9. J. K. Gimzewski, Ch. Gerber, E. Meyer, and R. R. Schlitter, *Chem. Phys. Lett.*, **217**, 589-594 (1994).
10. T. Thundat, R. J. Warmack, G. Y. Chen, and D. P. Allison, *Appl. Phys. Lett.*, **64**, 2894-2896 (1994).
11. E. A. Wachter, T. Thundat, P. G. Datskos, P. I. Oden, S. L. Sharp, and R. J. Warmack, "Remote Infrared Detection Using Microcantilevers", *Rev. Sci. Instrum.* (submitted).
12. G. Y. Chen, T. Thundat, E. A. Wachter, R. J. Warmack, "Adsorption-Induced Surface Stress and Its Effect on Resonance Frequency of Microcantilevers," *J. Appl. Phys.*, **77**, 1 (1995).
13. P.G. Datskos, P.I. Oden, T. Thundat, E.A. Wachter, R.J. Warmack and S.R. Hunter, "A Micromechanical Temperature Sensor", *Appl. Phys. Lett.* (submitted).
14. J. K. Gimzewski, Ch. Gerber, E. Meyer, and R. R. Schlitter, "Micromechanical Heat Sensor: Observation of a Chemical Reaction, Photon and Electrical Heat Pulses", in *Forces in Scanning Probe Methods*, Proceeding of the Nato ASI, H.-J. Güntherodt, D. Anselmetti, and E. Mayer (eds.) p. 123-131 (1995).
15. D. Sarid, *Scanning Force Microscopy*, Oxford University Press, New York, (1991).
16. "Investigations of the Reconstructed Gold Surface with Electrochemical Scanning Probe Microscopy" - PhD. dissertation, Patrick Ian Oden, Arizona State University Physics Department (1993).
17. P.I. Oden, N.J. Tao and S.M. Lindsay, *J. Vac. Sci. Technol.* **B11(2)**, 137 (1993).
18. Commercial versions available through Digital Instruments, Santa Barbara, CA and Park Scientific, Sunnyvale, CA.
19. W. C. Young, *Roark's Formulas for Stress and Strain*, Sixth ed., McGraw Hill, New York, pp. 118 (1989).
20. M. Tortorese, R. C. Barrett, and C. F. Quate, *Appl. Phys. Lett.*, **62**, 834 (1993).
21. F. J. Giessibl and B. M. Trafton, *Rev. Sci. Instrum.*, **65**, 1923 (1994).
22. Oriel Co., Model 43402 AMTIR-1 lens.
23. R. Anton, E.L Dereniak, and J. Garcia, *Infrared Technology XXI*, SPIE Vol. 2552, 592, July 1995.
24. N. Butler, R. Blackwell, R. Murphy, R. Silva, and C. Marshall, *Infrared Technology XXI*, SPIE Vol. 2552, 583, July 1995.
25. S. Fujii, T. Kamada, S. Hayashi, Y. Tomita, R. Takayama, T. Hirao, T. Nakayama, and T. Deguchi, *Infrared Technology XXI*, SPIE Vol. 2552, 612, July 1995.